Available online at www.sciencedirect.com

SCIENCE DIRECT

Polymer 46 (2005) 10945–10951

polymer

www.elsevier.com/locate/polymer

Crystallization, melting and morphology of PEO in PEO/MWNT-*g*-PMMA blends

Yeong-Tarng Shieh[a,*], Gin-Lung Liu[a], Kuo Chu Hwang[b], Chia-Chun Chen[c]

[a]*Department of Chemical Engineering, National Yunlin University of Science and Technology, Touliu, Yunlin 640, Taiwan, ROC*
[b]*Department of Chemistry, National Tsing Hua University, Hsinchu 300, Taiwan, ROC*
[c]*Department of Chemistry, National Taiwan Normal University, Taipei 116, Taiwan, ROC*

Received 3 March 2005; received in revised form 1 August 2005; accepted 7 September 2005
Available online 23 September 2005

Abstract

The dispersion of multi-walled carbon nanotubes (MWNTs) in crystalline poly(ethylene oxide) (PEO) is significantly improved by grafting with poly(methyl methacrylate) (PMMA) on surface of MWNTs via emulsion reactions. The synthesized MWNTs-*g*-PMMA is soluble in solvents that can dissolve PMMA and is well dispersed in PEO. The effects of the MWNTs-*g*-PMMA on PEO crystallization and its use as a reinforcement for PEO are investigated using DMA, DSC, POM, and SAXS. DMA data show that the PEO/MWNTs-*g*-PMMA blends containing up to 30 wt% MWNTs-*g*-PMMA are compatible. DSC data show the crystallization of PEO is enhanced by the MWNTs-*g*-PMMA, accompanying with a decreased thickness of crystal layers and an increased thickness of amorphous layers of the PEO lamellar stacks, in combination with SAXS data.

Keywords: Carbon nanotubes; Polymer composites; Crystallization

1. Introduction

Carbon nanotube has drawn much attention since its discovery in 1991 [1]. Carbon nanotube has a very high aspect ratio and very high Young's modulus [2–6]; therefore, it has been expected to be an excellent reinforcement for polymeric composites [7–9]. Without surface modifications, however, carbon nanotube aggregates in polymer matrix and gives poor reinforcing effects. In a previous report [10], we showed that carbon nanotube after grafting with poly(methyl methacrylate) (PMMA) could be well dispersed in commercial PMMA and significantly raise the storage modulus by ~1300% for the commercial PMMA containing 20 wt% of PMMA-grafted multiwalled carbon nanotubes (MWNTs) [10]. The tensile loading could effectively transfer to MWNTs because strong interactions were resulted between the PMMA matrix and the PMMA-grafted MWNTs.

This report presents a continuing study of the PMMA-grafted MWNTs (or MWNTs-*g*-PMMA) used as a reinforcement for a crystalline poly(ethylene oxide) (PEO) which has been a widely used material in both technological and particularly biomedical areas [11–14]. Since MWNTs-*g*-PMMA was found to have good dissolutions in those organic solvents that can dissolve PMMA, the MWNTs-*g*-PMMA are expected to uniformly disperse in the PEO matrix via the PMMA grafts of the MWNTs because the crystalline/amorphous PEO/PMMA blends have been reportedly compatible [15,16]. In this work, we attempt to see if the MWNTs-*g*-PMMA can also be an effective reinforcement for the crystalline PEO. The PEO/MWNTs-*g*-PMMA blends are thus, prepared by casting from chloroform solutions to investigate the reinforcing effects of the MWNTs-*g*-PMMA on PEO by a dynamic mechanical analyzer (DMA). Among the origins of the reinforcing effects, the morphology of PEO in the blends was emphatically investigated using differential scanning calorimetry (DSC), polarized optical microscopy (POM), and small angle X-ray scattering (SAXS).

2. Experimental

2.1. Synthesis and characterizations of MWNTs-g-PMMA

The multi-walled carbon nanotubes (MWNTs) obtained by the arc discharge method were purified for 3 h in a boiled

* Corresponding author.
E-mail address: shiehy@yuntech.edu.tw (Y.-T. Shieh).

0032-3861/$ - see front matter © 2005 Elsevier Ltd. All rights reserved.
doi:10.1016/j.polymer.2005.09.022

mixture of sulfuric acid and nitric acid in a composition of 3/2 by volume. During the acid purification, the MWNTs were carboxylated and used to synthesized MWNTs-*g*-PMMA by the emulsion polymerization method [10]. The grafting reactions of PMMA oligomer radicals onto MWNTs were in situ monitored by the electron spin resonance (ESR, Bruker, EMX-10, x-band). The grafting reactions were also examined by Fourier transform infrared spectroscopy (Bio-Rad FTIR, FTS 155). The content of PMMA in the MWNTs-*g*-PMMA samples was determined by the thermal gravimetric analyzer (TGA, TA instruments, TGA 2050). The glass transition temperature of the MWNTs-*g*-PMMA was measured by the differential scanning calorimeter (DSC, TA Instruments, DSC 2010) at a heating rate of 10 °C/min under nitrogen gas.

2.2. Preparations of PEO/MWNTs-g-PMMA blends

The PEO/MWNTs-*g*-PMMA blends with compositions of 100/0, 90/10, 80/20, and 70/30 were prepared by dissolving desired amounts of a commercial grade of PEO and the synthesized MWNTs-*g*-PMMA in chloroform to have the concentration of 1 g/100-cm^3 chloroform, followed by casting and vacuum drying at room temperature for two days. The cast films with $\sim$0.1 mm in thickness appeared to be uniform, showing a good dispersion of the MWNTs-*g*-PMMA in the PEO matrix. The commercial grade of PEO having $M_v = 900,000$ was acquired from Aldrich Chemical Company.

2.3. Characterizations of the PEO/MWNTs-g-PMMA blends

The dynamic mechanical properties of the blends were investigated by the dynamic mechanical analyzer (DMA, TA Instruments, DMA 2980) for rectangular samples with $\sim$0.1 mm in thickness. The DMA was measured in the tensile mode at a constant frequency of 1 Hz and a heating rate of 3 °C/min scanning from -120 to 100 °C.

The melting temperatures and degrees of crystallinities of the blends were measured by DSC. The samples were heated from room temperature to 150 °C at a heating rate of 10 °C/min, followed by cooling to room temperature and then heating again to 150 °C at the same rate. The melting temperatures and degrees of crystallinities of the blends were obtained from the second heating scans. The degrees of crystallinities of the blends were calculated by dividing the heats of fusion of samples by the heat of fusion of the perfectly crystalline PEO. The heat of fusion of the perfectly crystalline PEO is 205 J/g [17].

For Hoffman–Weeks plots, isothermal crystallizations of the blends were performed on the DSC by first heating the samples at a rate of 10 °C/min from room temperature to 150 °C holding for 10 min, followed by fast cooling to 40, 43, 45, 48, or 50 °C holding at each temperature for 0.5, 1, 3, 6, or 20 h, respectively. These isothermal crystallization times had been previously determined to be long enough for full crystallizations at these temperatures. In a typical preliminary experiment, the heat of fusion (ΔH) of a given sample after isothermal crystallization at a given temperature (T_c) was plotted as a function of isothermal time (t). The curve of this ΔH–t plot for a given sample was leveled off after a 'certain' time. This certain time was chosen for carrying out the isothermal crystallization. For a given sample, the leveled-off ΔH values (data not shown in this paper) are almost the same for all T_cs, suggesting that the levels of crystallinity were almost the same for all T_cs. The basis that was used to choose crystallization time in this work was the same as that extensively used in literature [18–20]. After isothermal crystallizations, the samples were cooled down to 30 °C and then heated at 10 °C/min to 100 °C to obtain heating endotherms. Melting temperatures (T_m) obtained from the endothermic peaks were plotted versus crystallization temperatures (T_c) for each sample. The equilibrium melting temperature T_m^0 of each sample was determined by the intersection of an extrapolation of the fitted line of each plot to the line of $T_m = T_c$.

To examine PEO isothermal crystallization rate on DSC, a sample was heated at a rate of 10 °C/min from room temperature to 150 °C holding for 10 min, followed by fast cooling to 45 or 50 °C, holding at each temperature for a desired time. After each isothermal crystallization for a desired time, the sample was heated from 45 or 50 to 100 °C to obtain heating endotherm. The endothermic enthalpy in joules per gram of PEO in each blend was calculated and plotted as a function of isothermal time.

Textures of spherulites of the samples after full crystallizations at 45 °C were investigated by a polarized optical microscopy (POM, Zeiss Axiolab A). Each sample was first melted in an oven followed by moving to the hot stage at 45 °C for full crystallizations.

Weight-average long periods (the weight average of the sums of thickness of the crystal and amorphous layers in lamellar stacks) of the blends were investigated by a small angle X-ray scattering (SAXS). All SAXS measurements were performed at room temperature for samples after fully crystallized at 45 °C. The X-ray source was operated at 200 mA and 40 kV and was generated by an 18 kW rotating anode X-ray generator (Rigaku) with a rotating anode Cu target. The incident X-ray beam was monochromated by a pyrolytic graphite and a set of three pinhole inherent collimators was used so that the smearing effects inherent in slit-collimated small-angle X-ray cameras can be avoided. The sizes of the first and second pinhole are 1.5 and 1.0 mm, respectively, and the size of the guard pinhole before the sample is 2.0 mm. The scattered intensity was detected by a two-dimensional position sensitive detector (Ordela Model 2201X, Oak Ridge Detector Laboratory Inc.) with 256×256 channels (active area 20×20 cm^2 with $\sim$1 mm resolution). The sample to detector distance is 4000 mm long. The beam stop is around lead disk of 18 mm in diameter. All data were corrected by the background (dark current and empty beam scattering) and the sensitivity of each pixel of the area detector. The area scattering pattern has been radially averaged to increase the efficiency of data collection compared with one-dimensional linear detector. Data were acquired and processed on an IBM-compatible personal computer.

3. Results and discussion

FTIR and ESR data revealed that PMMA had been successfully grafted onto MWNTs to form PMMA-grafted MWNTs (or MWNTs-*g*-PMMA) in our previous report [10]. The amount of the PMMA grafts on MWNTs was ~39 wt% of the total weight of the synthesized MWNTs-*g*-PMMA as measured by TGA [10]. Although the molecular weight of the grafted PMMA is unknown, it is lower than that of the commercial PMMA, as suggested by glass transition temperature data. As can be seen in Fig. 1, T_g of the MWNTs-*g*-PMMA is ~88 °C while that of the commercial PMMA, normally having a molecular weight of hundreds of thousand grams per mole, is ~108 °C. The lower T_g suggests that the molecular weight of the PMMA grafts on MWNTs is not very high.

The grafting reactions are also confirmed by the formation of a homogeneous solution of the MWNTs-*g*-PMMA in chloroform without precipitation for a long period of time whereas precipitation is observed in a short period of time for the ungrafted MWNTs. Additional supporting evidence (pictures not shown in this paper) is that homogeneous films are obtained for the PEO/MWNTs-*g*-PMMA blends of various compositions while the ungrafted MWNTs give aggregated clusters in the films. Without grafting modifications, MWNTs aggregate, even with the aid of prolonged sonication, to form heterogeneous morphology whereas, with grafting modifications, the MWNTs-*g*-PMMA are uniformly dispersed in the PEO matrix.

The uniform films of PEO/MWNTs-*g*-PMMA blends as prepared by casting from chloroform solutions are investigated by DMA measurements. Fig. 2 shows composition variations of loss moduli for four samples as a function of temperature. As can be seen from Fig. 2, each loss modulus curve exhibits only one peak. In other words, each sample exhibits one T_g, an indication of a compatible blend in the amorphous phase [21,22]. The T_g of the blends apparently increases with increasing content of MWNTs-*g*-PMMA, having a much higher T_g (~88 °C) as compared with PEO having T_g of about −60 °C [16]. According

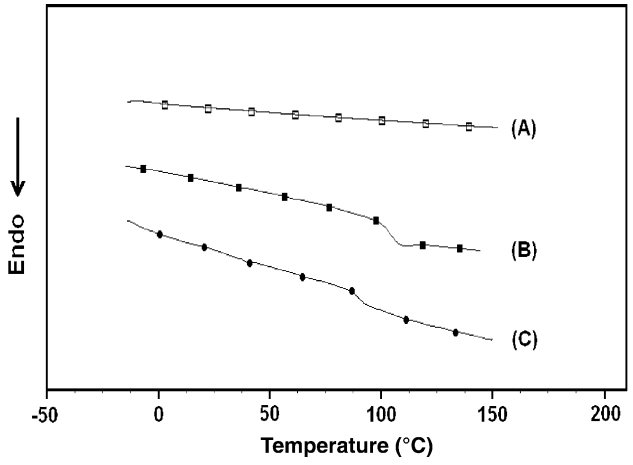

Fig. 1. DSC heating scans for (A) MWNTs, (B) commercial PMMA, (C) MWNTs-*g*-PMMA. The MWNTs-*g*-PMMA contains about 39 wt% of PMMA as measured by a TGA.

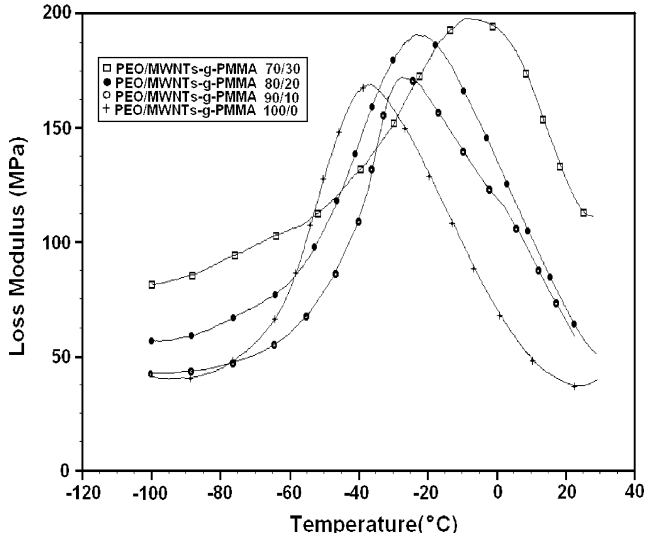

Fig. 2. Loss modulus curves of DMA as a function of temperature for + PEO/MWNTs-*g*-PMMA 100/0; ○ PEO/MWNTs-*g*-PMMA 90/10; ● PEO/MWNTs-*g*-PMMA 80/20; □ PEO/MWNTs-*g*-PMMA 70/30.

to literature [23–31], when the unmodified MWNTs content is over a few weight percents, the MWNTs would form aggregations in polymer composites, even with the aid of surfactants for their dispersion. The DMA data here thus, can serve as additional supporting evidence that grafting modifications on MWNTs can improve dispersion of the MWNTs in the PEO matrix because poor dispersion of MWNTs in the polymer matrix would result in phase separations and multiple T_gs.

Table 1 tabulates composition variations of melting temperatures, heats of fusion, and weight fractional crystallinities of the PEO/MWNTs-*g*-PMMA blends. As can be seen in Table 1, the incorporation of MWNTs-*g*-PMMA depresses melting temperatures but enhances crystallinities of PEO in the blends. The 10 wt% incorporation of MWNTs-*g*-PMMA exhibits the most significant enhancement of the PEO crystallinity. This is not seen from the PEO/PMMA blends [21]. The amorphous PMMA component would depress both melting temperature and crystallinity of the crystalline PEO component [32].

The depression of melting temperature of a crystalline polymer in a binary blend by the other polymer component which is amorphous arises from two sources [33]: (i) the dilution

Table 1
Melting temperatures (T_m, °C), heats of fusion (ΔH, J/g), and weight fractional crystallinities (w_c, %) of PEO/MWNTs-*g*-PMMA blends

PEO/MWNTs-*g*-PMMA	T_m	ΔH (J/g blend)	ΔH (J/g PEO)	w_c [a]
100/0	67.8	120.0	120.0	58.5
90/10	63.1	125.9	139.9	68.2
80/20	62.0	108.9	136.1	66.4
70/30	57.7	95.1	135.9	66.3

[a] The weight fractional crystallinities of PEO were calculated by dividing the heat of fusion, ΔH, in joules per gram PEO in a blend sample by ΔH^0, which is 205 J/g for perfectly crystalline PEO [17].

effect in the amorphous phase. This dilution effect will lower chemical potential of PEO at the melt of the blend than that in the pure state to cause the depression of melting temperature; (ii) the morphological change (namely, change in crystal thickness) of the crystalline component due to the presence of the other component in the blend. The latter source depends on the interfacial energy between the crystal and the amorphous phases and obviously depends on the composition and the crystallization rate of the blend. Although the composition variation of melting temperature and crystallinity in opposite direction implies that the dilution effect and morphological effect may be both present in the blends, more evidence is needed to confirm their presence. Equilibrium melting temperature (T_m^0) of the infinitely thick PEO crystal [34] and the thickening factor (γ) of PEO crystallization in the PEO/MWNTs-*g*-PMMA blends are thus, investigated. For determining (T_m^0) of a crystalline polymer, the equation of Hoffman and Weeks [35] as in Eq. (1) is usually applied, by which the intersection of an extrapolation of the experimental melting temperature, T_m, versus crystallization temperature, T_c, with the diagonal line of $T_m = T_c$ is taken as (T_m^0). The (T_m^0) can also be obtained by measuring the lamellar thickness l_c by small-angle X-ray scattering; then, plotting T_m against $1/l_c$ and extrapolating to zero. This intercept should also yield the (T_m^0) of the infinitely thick crystal [34].

$$T_m = T_m^0\left(1-\frac{1}{\gamma}\right)+\frac{T_c}{\gamma} \quad (1)$$

Fig. 3 shows Hoffman–Weeks plots for the PEO/MWNTs-*g*-PMMA blends. The (T_m^0) and the thickening factor obtained from Hoffman–Weeks plots are tabulated in Table 2. As can be seen from Table 2, (T_m^0) of pure PEO is 71.5 °C. (T_m^0) of the 90/10 blend is 73 °C and is decreased by increasing content of MWNTs-*g*-PMMA. The morphological effect can be characterized by the thickening factor [36,37], γ, which is the ratio of the final thickness of crystallite lamella to the initial thickness at beginning of crystallization. In general, the value of γ can be calculated from the slope of Hoffman–Weeks plot, because it is the reciprocal of the slope related by Eq. (1). As can be seen from

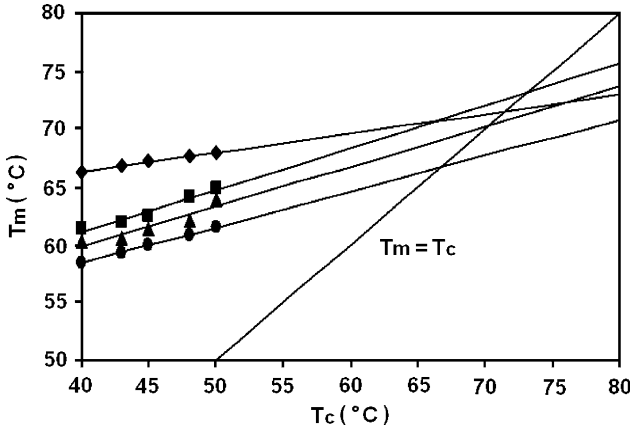

Fig. 3. Hoffman–Weeks plots for ♦ PEO/MWNTs-*g*-PMMA 100/0; ■ PEO/MWNTs-*g*-PMMA 90/10; ▲ PEO/MWNTs-*g*-PMMA 80/20; ● PEO/MWNTs-*g*-PMMA 70/30.

Table 2
Equilibrium melting temperatures and thickening factors of the PEO/MWNTs-*g*-PMMA blends as determined from Hoffman–Weeks plots

PEO/MWNTs-*g*-PMMA	100/0	90/10	80/20	70/30
T_m^0, (°C)	71.5	73	70	67
γ	6.01	2.73	2.88	3.22
$T_m^0/(T_m^0 - T_m)$	19.3	7.4	8.8	7.2

Table 2, the γ value measured for PEO is decreased by adding 10 wt% of MWNTs-*g*-PMMA, implying a depression of T_m [35], consistent with the experimental result. With increasing MWNTs-*g*-PMMA content beyond 10-wt% of MWNTs-*g*-PMMA, the γ value of PEO is slightly increased, along with decreases of both T_m and (T_m^0) of PEO (Tables 1 and 2). This inconsistent variation of γ with T_m would imply that the variation of γ value gives insignificant effect on the depression of T_m and (T_m^0) of PEO in PEO/MWNTs-*g*-PMMA blends. In other words, beyond 10 wt% of MWNTs-*g*-PMMA, the composition variation of T_m and (T_m^0) of PEO is mainly attributed to the dilution effect of the other component in the blends other than the morphological effect [36,37].

According to the Thomson–Gibbs equation [38], crystal thickness (l_c), and melting temperature (T_m) are correlated as in Eq. (2):

$$T_m = T_m^0\left(1-\frac{2\sigma}{l_c\rho_c\Delta H}\right) \quad (2)$$

where (T_m^0) is the equilibrium melting temperature, ρ_c is the mass density of the crystal, ΔH is the equilibrium heat of fusion/unit weight, and σ is the surface free energy. Eq. (2) can be rearranged as in Eq. (3).

$$l_c = \frac{2\sigma T_m^0}{\rho_c \Delta H (T_m^0 - T_m)} \quad (3)$$

Eq. (3) prescribes that the crystal thickness (l_c) is proportional to $T_m^0/(T_m^0 - T_m)$, since, ρ_c and σ are constants and if ΔH is assumed to be an insignificant function of composition of a crystalline/amorphous blend. $T_m^0/(T_m^0 - T_m)$ can thus, serve as a measure for composition variation of l_c. As also tabulated in Table 2, the size of l_c is significantly decreased by an incorporation of MWNTs-*g*-PMMA. Thus, the increase of PEO crystallinity by MWNTs-*g*-PMMA suggests that PEO gives more in the number of smaller crystals as a result of incorporation of MWNTs-*g*-PMMA.

In an attempt to further investigate the enhancement of PEO crystallization upon incorporation of MWNTs-*g*-PMMA, isothermal crystallizations of samples are conducted on DSC at 45 or 50 °C for a certain time, followed by heating up to 100 °C to obtain heating endotherms. Fig. 4 exhibits heats of fusion in joules per gram PEO after isothermal crystallizations of samples at 45 or 50 °C as plotted as a function of isothermal time. As can be seen in Fig. 4, the crystallization rates are fast initially and level off in the later stage. It is clear that the 10-wt% incorporation of MWNTs-*g*-PMMA significantly enhances PEO crystallization at both temperatures while the 20 wt% incorporation gives a less extent of enhancement for

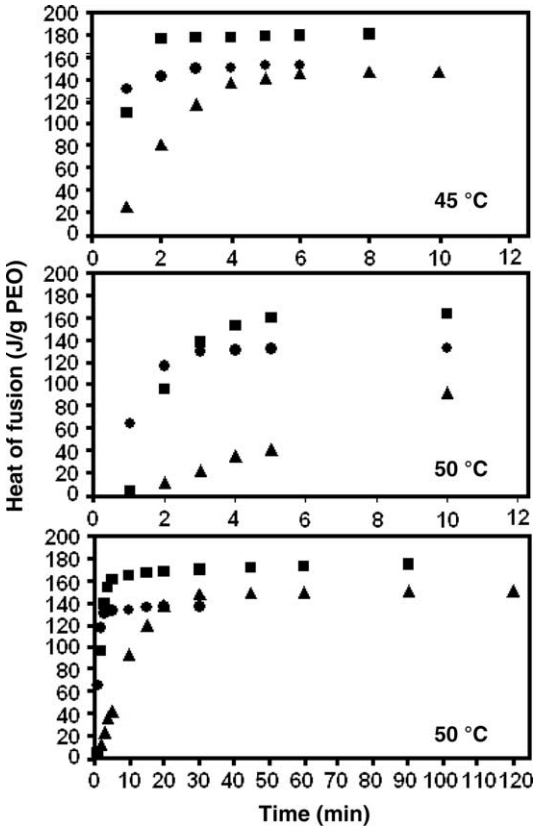

Fig. 4. Heats of fusion of PEO after isothermal crystallizations at 45 and 50 °C for various times for ● PEO/MWNTs-*g*-PMMA 100/0; ■ PEO/MWNTs-*g*-PMMA 90/10; ▲ PEO/MWNTs-*g*-PMMA 80/20. The bottom two graphs are the same except the scale in *x* axis.

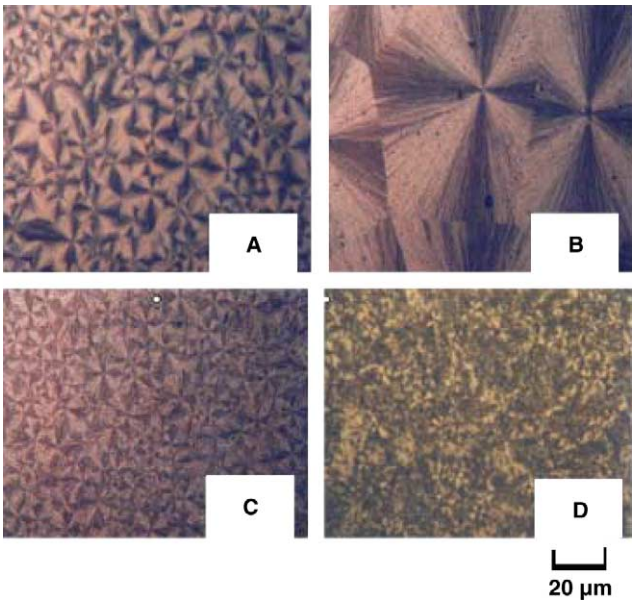

Fig. 5. Polarized optical microscopy images of PEO/MWNTs-*g*-PMMA blends after isothermal crystallizations at 45 °C: (A) PEO/MWNTs-*g*-PMMA 100/0; (B) PEO/MWNTs-*g*-PMMA 90/10; (C) PEO/MWNTs-*g*-PMMA 80/20; (D) PEO/MWNTs-*g*-PMMA 70/30.

the 50 °C crystallization and an insignificant enhancement for the 45 °C crystallization as can be seen by the leveled-off heats of fusion. Fig. 5 shows POM images of pure PEO and three PEO/MWNTs-*g*-PMMA blends. In Fig. 5, volume filling spherulites can be seen for pure PEO and the PEO blends containing 10 and 20 wt% of MWNTs-*g*-PMMA whereas spherulites can not be clearly seen for the blend containing 30 wt% MWNTs-*g*-PMMA. As compared with pure PEO, the bigger sizes of spherulites for the PEO/MWNTs-*g*-PMMA 90/10 blend suggest that the MWNTs-*g*-PMMA serves as a nucleating agent for the crystallization resulting in higher crystallinity as supported by DSC data in Fig. 4. As compared with the PEO/MWNTs-*g*-PMMA 90/10 blend, the PEO/MWNTs-*g*-PMMA 80/20 blend gives smaller sizes of spherulites because of more nanotubes in the blends serving as nucleating agents. The PEO/MWNTs-*g*-PMMA 70/30 blend gives unclear spherulites because of too much amount of the amorphous MWNTs-*g*-PMMA in the blend.

Fig. 6 shows the Lorentz-corrected SAXS profiles (Iq^2 vs q) of pure PEO and three PEO/MWNTs-*g*-PMMA blends after isothermal crystallizations at 45 °C. The electron densities of crystalline PEO, amorphous PEO, and PMMA calculated from their mass densities (1.24, 1.12, and 1.19 g/cm^3, respectively), are 0.676, 0.612, and 0.642 mol/cm^3, respectively. As can be seen in Fig. 6, the scattering intensity of the samples decreases with increasing content of the MWNTs-*g*-PMMA suggesting that the MWNTs-*g*-PMMA is present in the interlamellar regions, as this would decrease the electron density contrast between the crystalline and amorphous layers in the lamellar stacks.

The weight-average long period associated with the lamellar stacks can be calculated from the peak maximum of the Lorentz-corrected SAXS profiles using the Bragg's equation, $L=2\pi/q_{max}$. The composition variations of long periods ranging from 47.9 nm for pure PEO to 56.6 nm for the PEO/MWNTs-*g*-PMMA 70/30 blend are tabulated in Table 3. The long period of the PEO lamellar stacks is apparently increased by adding MWNTs-*g*-PMMA. This increase in long period enlarges with increasing content of MWNTs-*g*-PMMA until 20 wt% beyond which the increase turns out to be insignificant. In the lamellar stack model with sharp phase boundary, the long period represents the sum of the crystal thickness (l_c) and the amorphous layer thickness (l_a). Rise in long period may thus, stem from the thickening of crystal layer or the swelling of amorphous layer.

The one-dimensional correlation function may be utilized to deconvolute long period into the thickness of these two types of layers. The correlation function, $K(z)$, defined by Strobl and Schneider, adopts the following form [39]:

$$K(z) = \frac{1}{2\pi^2}\int_0^\infty I(q)q^2\cos(qz)\mathrm{d}q \quad (4)$$

where $I(q)$ is the absolute scattering intensity obtained from the SAXS measurement, $q=4\pi/\lambda\sin(\theta/2)$ (θ=scattering angle), and z is the direction along which the electron density is measured. In this study, attributed to low q_{max} values in

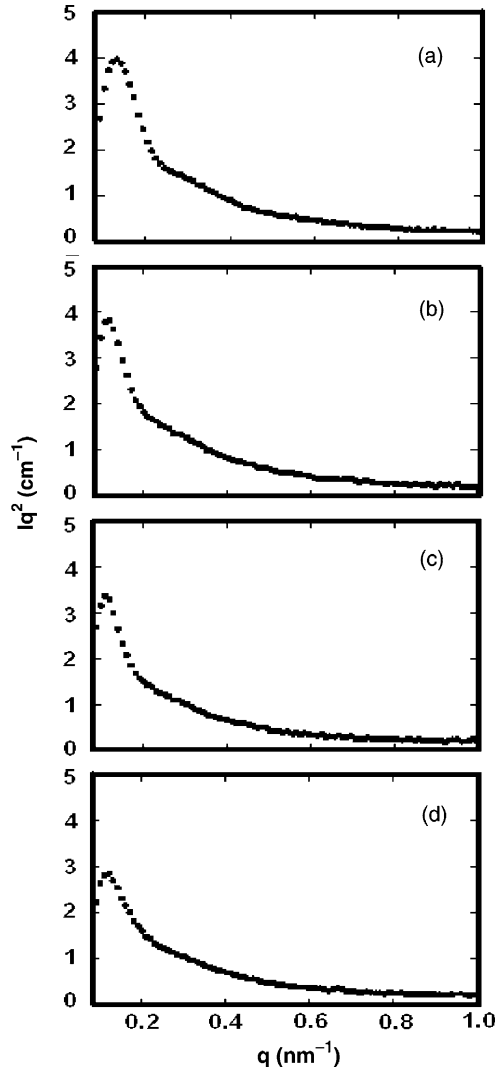

Fig. 6. Lorentz-corrected SAXS profiles of (a) pure PEO, (b) PEO/MWNTs-*g*-PMMA 90/10, (c) PEO/MWNTs-*g*-PMMA 80/20, (d) PEO/MWNTs-*g*-PMMA 70/30 blends after isothermal crystallizations at 45 °C.

the Lorentz-corrected SAXS profiles of pure PEO and its blends, the reliable one-dimentional correlation function was not obtained from the SAXS conditions used because when the integration of Eq. (4) was performed, the extrapolation to zero q using the Debye–Bueche model [40,41] has resulted in a big error. Although the long periods ($L=l_c+l_a$) cannot be successfully deconvoluted into thickness of crystal layer (l_c) and thickness of amorphous layer (l_a), the increase of the long periods with increasing MWNTs-*g*-PMMA content is

Table 3
The q_{max} of Lorentz-corrected SAXS profiles and long periods ($L=2\pi/q_{max}$) of the PEO/MWNTs-*g*-PMMA blends

PEO/MWNTs-*g*-PMMA	q_{max}	L, (nm)
100/0	0.1312	47.9
90/10	0.1211	51.9
80/20	0.1110	56.6
70/30	0.1110	56.6

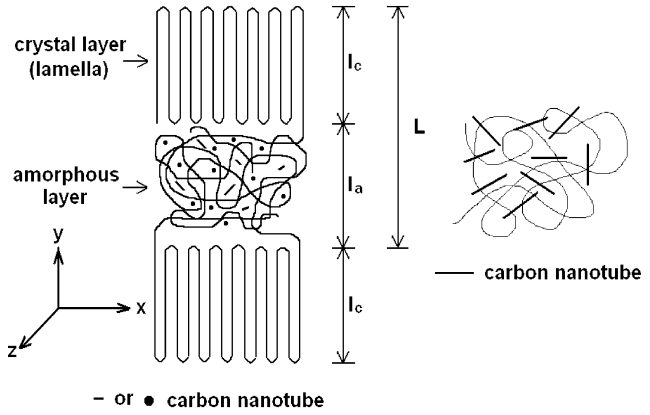

Fig. 7. A schematic representation of the nanotubes in the amorphous layer in between two crystal lamellae in a lamellar stack as represented by the left part of the above figure, where l_c is the thickness of the crystal layer, l_a the thickness of the amorphous layer and L ($=l_c+l_a$) the long period. The nanotubes are axially parallel to the two crystal lamellae in the lamellar stack. The left part of the above figure is a vertical view (i.e. z-direction) to the polymer main chains in the crystal lamellae while the right part of the figure is a view parallel (i.e. y-direction) to the polymer main chains in the crystal lamellae.

suggested to be attributed to the swelling of the amorphous layer because of decreasing crystal size with increasing MWNTs-*g*-PMMA content as can be inferred by DSC data previously. The MWNTs-*g*-PMMA, staying in the amorphous layer, is suggested to be axially parallel to two crystal lamellae between which the amorphous layer is located, because the length of the MWNTs of hundreds or thousands of nanometers is much larger than the thickness of the amorphous layer of only tens of nanometer as schematically represented in Fig. 7.

In an attempt to examine the reinforcing effects of the MWNTs-*g*-PMMA on PEO, dynamic mechanical properties of the PEO composites were measured by the dynamic mechanical analyzer (DMA). As can be seen from Fig. 8,

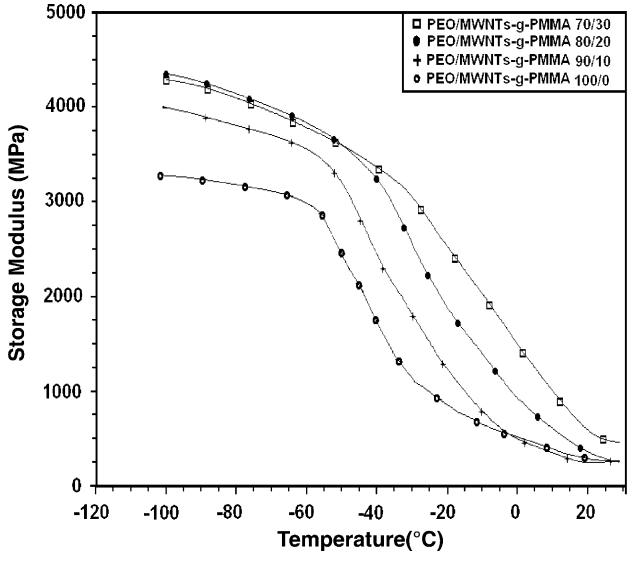

Fig. 8. Storage modulus curves of DMA as a function of temperature for ○ PEO/MWNTs-*g*-PMMA 100/0; + PEO/MWNTs-*g*-PMMA 90/10; ● PEO/MWNTs-*g*-PMMA 80/20; □ PEO/MWNTs-*g*-PMMA 70/30.

below −50 °C the storage modulus of the PEO/MWNTs-*g*-PMMA composite increases with increasing content of the MWNTs-*g*-PMMA up to 20 wt%. The storage modulus at −100 °C, which is below T_g of pure PEO, was up ~38% from ~3.2 GPa for pure PEO to ~4.4 GPa for the composite containing 20 wt% MWNTs-*g*-PMMA. The reinforcement of the storage modulus of PEO after the addition of MWNTs-*g*-PMMA is associated with the PMMA grafts, which are compatible with PEO molecules, on the MWNTs walls. These PMMA grafts can physically knot and tangle together with PEO polymer chains in the matrix, leading to strong overall interactions of the MWNTs and the matrix. MWNTs thus, serve as the network centers to transfer local stress evenly to all other polymer chains. The mechanical properties of the PEO composite can thus be improved. The reinforcement of mechanical properties of PEO by MWNTs-*g*-PMMA is moderate. The reinforcing effects of the MWNTs-*g*-PMMA on PEO matrix are not as high as those on PMMA matrix. Martuscelli and coworkers [42,43] have studied the interaction between PEO and PMMA using FTIR and found a very weak Van der Waals type interaction between them. The compatibility of the PEO/PMMA was more 'physical' than 'chemical'. In the previous study [10], the interactions between high-molecular-weight PMMA matrix and the PMMA grafts on the MWNTs, however, are strong, as can be inferred from the high T_g value of PMMA. In PMMA/MWNTs-*g*-PMMA blends, the PMMA grafts on the MWNTs walls can completely 'dissolve' in the PMMA matrix which is a totally amorphous polymer. In this study, the PMMA grafts on the MWNTs, however, stay only in the amorphous layer in between two PEO lamellae layers (Fig. 7). Furthermore, although the MWNTs-*g*-PMMA can enhance the PEO crystallinities, it results in decreased thickness of crystal layers leading to moderate reinforcing effects on PEO. Thus, carbon nanotube as a reinforcement for a crystalline polymer may not be as effective as that for an amorphous polymer. To drastically reinforce a crystalline polymer with MWNTs, the choice of crystalline polymer grafts that can co-crystallize with the crystalline matrix might be needed. Experiments are under way to examine such a hypothesis.

4. Conclusions

The incorporation of PMMA-grafted MWNTs can enhance PEO crystallization, leading to moderate reinforcing effects on PEO. In a previous work, the PMMA-grafted MWNTs showed significant reinforcing effects on totally amorphous PMMA. The high aspect ratio of carbon nanotube used as a reinforcement for a crystalline polymer (the nanotubes are confined in the amorphous layers of the lamellar stacks) might not be as effective as that for a totally amorphous polymer (the nanotubes dissolve uniformly in whole amorphous matrix).

Acknowledgements

The authors are grateful to the financial support from National Science Council of Taiwan under contract NSC 92-2216-E-224-004.

References

[1] Iijima S. Nature 1991;354:56.
[2] Yu MF, Lourie O, Dyer MJ, Moloni K, Kelley TF, Ruoff RS. Science 2000;287:637.
[3] Yu MF, Files BS, Arepalli S, Rouff RS. Phys Rev Lett 2000;84:5552.
[4] Yu MF, Yakobson BI, Ruoff RS. J Phys Chem B 2000;104:8764.
[5] Krishnan A, Dujardin E, Ebbesen TW, Yianilos PN, Treacy MMJ. Phys Rev B 1998;58:14013.
[6] Poncharal P, Wang ZL, Ugarte D, de Heer WA. Science 1999;283:1513.
[7] Calvert P. Nature 1999;399:210.
[8] Service RF. Science 1998;281:940.
[9] Dagani R. C&EN 1999;June 7:25.
[10] Hwang GL, Shieh Y-T, Hwang KC. Adv Funct Mater 2004;14(5):487.
[11] Harris JM. Poly(ethylene glycol) chemistry: biotechnical and biomedical application. New York: Plenum Press; 1992.
[12] Blin J-L, Léonard A, Yuan Z-Y, Gigot L, Vantomme A, Cheetham AK, et al. Angew Chem Int Ed 2003;42:2872.
[13] Maggi L, Segale L, Torre ML, Machiste EO, Conte U. Biomaterials 2002; 23:1113.
[14] Ryan PL, Foty RA, Kohn J, Steinberg MS. Proc Natl Acad Sci USA 2001; 98:4323.
[15] Martuscelli E, Pracella M, Wang PY. Polymer 1984;25:1097.
[16] Shieh Y-T, Liu K-H, Lin T-L. J Supercritical Fluids 2004;28(1):101–12.
[17] Vidotto G, Levy DL, Kovacs AJ. Kolloid-Z Z Polym 1968;230:299.
[18] Nandi AK, Mandelkern L. J Polym Sci, Polym Phys Ed 1991;29:1287.
[19] Maiti P, Nandi AK. Macromolecules 1995;28:8511.
[20] Shieh Y-T, Lee M-S, Chen S-A. J Polym Sci, Polym Phys Ed 2002;40: 638.
[21] Li X, Hsu SL. J Polym Sci, Part B: Polym Phys Ed 1984;22:1331.
[22] Liberman SA, Gomes AS, Macki EM. J Polym Sci, Part A: Polym Chem Ed 1984;22:2809.
[23] Ajayan PM, Stephean O, Lolliex C, Trauth D. Science 1998;265:1212.
[24] Schadler LS, Gianmaris SC, Ajayan PM. Appl Phys Lett 1998;73:3842.
[25] Curran SA, Ajayan PM, Blau WJ, Carroll DL, Coleman JN, Dalton AB, et al. Adv Mater 1998;10:1091.
[26] Ajayan PM, Schadler LS. Adv Mater 2000;12:750.
[27] Jia Z, Wang Z, Xu C, Liang J, Wei B, Wu D, et al. Mater Sci Eng 1999; A271:395.
[28] Gong X, Liu J, Baskaran S, Voise RD, Young JS. Chem Mater 2000;12: 1049.
[29] Haggenmueller R, Gommans HH, Rinzler AG, Fisher JE, Winey KI. Chem Phys Lett 2000;330:219.
[30] Shaffer MSP, Windle AH. Adv Mater 1999;11:937.
[31] Qian D, Dickey EC, Andrews R, Rantell T. Appl Phys Lett 2000;76:2868.
[32] Parizel N, Laupretre F, Monnerie L. Polymer 1997;38:3719.
[33] Harrison IR, Runt J. J Polym Sci, Polym Phys Ed 1980;18:2257.
[34] Stein RS. J Polym Sci, Polym Phys Ed 1981;19:1281.
[35] Hoffman JD, Weeks JJ. J Res Natl Bur Stand 1962;66:13.
[36] Nishi T, Wang TT. Macromolecules 1975;8:909.
[37] Rim PB, Runt JP. Macromolecules 1984;17:1520.
[38] Gedde UW. Polymer physics. New York: Chapman and Hall; 1995.
[39] Strobl GR, Schneider M. J Polym Sci, Polym Phys Ed 1980;18:1343.
[40] Debye P, Bueche AM. J Appl Phys 1949;20:518.
[41] Debye P, Anderson Jr HR, Brumberger H. J Appl Phys 1957;28:679.
[42] Martuscelli E, Pracella M, Yue WP. Polymer 1984;25:1097.
[43] Rao GR, Castiglioni C, Gussoni M, Zerbi G, Martuscelli E. Polymer 1985;26:811.